

This is a repository copy of *Quantitative In-situ Monitoring of Parahydrogen Fraction Using Raman Spectroscopy*.

White Rose Research Online URL for this paper:

<https://eprints.whiterose.ac.uk/134335/>

Version: Accepted Version

---

**Article:**

Parrott, Andrew J., Dallin, Paul, Andrews, John et al. (5 more authors) (2019) Quantitative In-situ Monitoring of Parahydrogen Fraction Using Raman Spectroscopy. APPLIED SPECTROSCOPY. pp. 88-97. ISSN 0003-7028

<https://doi.org/10.1177/0003702818798644>

---

**Reuse**

Items deposited in White Rose Research Online are protected by copyright, with all rights reserved unless indicated otherwise. They may be downloaded and/or printed for private study, or other acts as permitted by national copyright laws. The publisher or other rights holders may allow further reproduction and re-use of the full text version. This is indicated by the licence information on the White Rose Research Online record for the item.

**Takedown**

If you consider content in White Rose Research Online to be in breach of UK law, please notify us by emailing [eprints@whiterose.ac.uk](mailto:eprints@whiterose.ac.uk) including the URL of the record and the reason for the withdrawal request.

# Quantitative In-situ Monitoring of Parahydrogen Fraction Using Raman Spectroscopy

Journal Title  
XX(X):1-9  
©The Author(s) 2018  
Reprints and permission:  
sagepub.co.uk/journalsPermissions.nav  
DOI: 10.1177/ToBeAssigned  
www.sagepub.com/

SAGE

Andrew J. Parrott<sup>1</sup>, Paul Dallin<sup>2</sup>, John Andrews<sup>2</sup>, Peter M. Richardson<sup>3</sup>, Olga Semenova<sup>3</sup>, Meghan E. Halse<sup>3</sup>, Simon B. Duckett<sup>3</sup>, and Alison Nordon<sup>1</sup>

## Abstract

Raman spectroscopy has been used to provide a rapid, non-invasive and non-destructive quantification method for determining the parahydrogen fraction of hydrogen gas. The basis of the method is the measurement of the ratio of the first two rotational bands of hydrogen at  $355\text{ cm}^{-1}$  and  $586\text{ cm}^{-1}$  corresponding to parahydrogen and orthohydrogen, respectively. The method has been used to determine the parahydrogen content during a production process and a reaction. In the first example, the performance of an in-house liquid nitrogen cooled parahydrogen generator was monitored both at-line and on-line. The Raman measurements showed that it took several hours for the generator to reach steady state and hence, for maximum parahydrogen production (50 %) to be reached. The results obtained using Raman spectroscopy were compared to those obtained by at-line low-field NMR spectroscopy. While the results were in good agreement, Raman analysis has several advantages over NMR for this application. The Raman method does not require a reference sample, as both spin isomers (ortho and para) of hydrogen can be directly detected, which simplifies the procedure and eliminates some sources of error. In the second example, the method was used to monitor the fast conversion of parahydrogen to orthohydrogen in-situ. Here the ability to acquire Raman spectra every 30 s enabled a conversion process with a rate constant of  $27.4 \times 10^{-4}\text{ s}^{-1}$  to be monitored. The Raman method described here represents an improvement on previously reported work, in that it can be easily applied on-line and is approximately 500 times faster. This offers the potential of an industrially compatible method for determining parahydrogen content in applications that require the storage and usage of hydrogen.

## Keywords

Raman spectroscopy, quantitative analysis, in-situ monitoring, gas analysis, hydrogen, parahydrogen

## Introduction

Molecular hydrogen ( $\text{H}_2$ ) exists as two nuclear spin isomers: the antisymmetric singlet nuclear spin state parahydrogen ( $\text{pH}_2$ ) and the symmetric triplet spin nuclear state orthohydrogen ( $\text{oH}_2$ ). The equilibrium distribution of the two isomers is a function of temperature. At room temperature, the equilibrium composition is approximately 25 %  $\text{pH}_2$  and 75 %  $\text{oH}_2$ , a mixture typically referred to as normal hydrogen ( $\text{nH}_2$ ). At lower temperatures the equilibrium distribution shifts to favour the lower energy  $\text{pH}_2$  isomer, so that at its boiling point (20.3 K) the equilibrium composition of  $\text{H}_2$  is almost 100 %  $\text{pH}_2$ . However, as the conversion between  $\text{oH}_2$  and  $\text{pH}_2$  is forbidden, conversion between isomers is very slow unless a catalyst is used.<sup>1-5</sup>

The  $\text{pH}_2$  isomer is useful for a wide range of applications, including: liquid fuels,<sup>6-8</sup> matrix isolation spectroscopy,<sup>9,10</sup> certain hyperpolarisation methods for nuclear magnetic resonance (NMR) spectroscopy,<sup>3,4,11,12</sup> and as a moderator for spallation neutron sources.<sup>13,14</sup> For many of these applications the proportion of the  $\text{pH}_2$  isomer is of vital importance. For example, for fuel applications  $\text{H}_2$  is usually stored as a liquid. If the  $\text{oH}_2$  is not fully converted to  $\text{pH}_2$  (e.g. by passing over a suitable catalyst) before condensation from the gas state, then the slow exothermic conversion of  $\text{oH}_2$  to  $\text{pH}_2$  will liberate enough heat to vaporise up to 64 %

of the liquid.<sup>7</sup> For  $\text{pH}_2$  based hyperpolarisation methods in NMR, the greater the level of  $\text{pH}_2$  enrichment the greater the NMR signal enhancement.<sup>4,11,15</sup> Indeed various methods of generating high purity  $\text{pH}_2$  for NMR studies have been reported,<sup>15,16</sup> and major NMR vendors also supply this type of specialised equipment.<sup>17</sup>

The research group at the University of Strathclyde has an in-house built  $\text{pH}_2$  generator, which is used to provide gaseous  $\text{pH}_2$  for signal amplification by reversible exchange (SABRE) hyperpolarisation studies on a bench-top NMR spectrometer.<sup>18-20</sup> To validate the hyperpolarisation experiments, it is desirable to be able to rapidly monitor the  $\text{pH}_2$  fraction produced by this generator. The two spin isomers differ slightly in several physical properties, such as: heat capacity, vapour pressure, speed of sound,

<sup>1</sup>WestCHEM, Department of Pure and Applied Chemistry and CPACT, University of Strathclyde, Glasgow, UK

<sup>2</sup>Clairet Scientific Ltd., Northampton, UK

<sup>3</sup>Centre for Hyperpolarisation in Magnetic Resonance (CHyM), Department of Chemistry, University of York, York, UK

## Corresponding author:

Andrew J. Parrott and Alison Nordon, WestCHEM, Department of Pure and Applied Chemistry and CPACT, University of Strathclyde, Glasgow, UK.

Email: andrew.parrott@strath.ac.uk, alison.nordon@strath.ac.uk

and thermal conductivity. These properties can be used to measure the  $p\text{H}_2$  enrichment in an unknown sample.<sup>4,9,21–23</sup> Nevertheless, many of these measurements often require that other parameters also be measured very accurately (e.g. temperature and pressure), and require calibration with known mixtures to provide quantitative results.<sup>15,21,24</sup> However, as the two spin isomers occupy different rotational energy levels,<sup>1,3,4,25</sup> it is possible to use Raman spectroscopy to probe the rotational transitions of  $\text{H}_2$  gas, and hence determine the composition of  $p\text{H}_2$  without calibration mixtures.<sup>8,13,14,25,26</sup>

In the context of monitoring  $p\text{H}_2$  enrichment, Sundararajan et al.<sup>10</sup> used a Raman microscope with a 514 nm laser for off-line monitoring of  $\text{H}_2$  gas used for matrix isolation spectroscopy. They reported that even with 1000 scans, the analysis could not be conducted quantitatively. Teshigawara et al.<sup>14</sup> used a Raman microscope for off-line monitoring of  $\text{H}_2$  moderators in a neutron source. They did not report the analysis time, but did claim that sufficient signal was obtained for quantitative analysis. Matthews et al.<sup>8,26</sup> reported the use of a specialised gas cell for off-line monitoring of  $\text{H}_2$  gas from a liquid hydrogen storage tank. They used a 532 nm laser and reported an integration time of only 60 s. However, the density of the gas measured (and hence pressure) was much higher ( $>12 \text{ g L}^{-1}$ ) than typically produced by the  $p\text{H}_2$  generator used here ( $<0.5 \text{ g L}^{-1}$ ). Sutherland et al.<sup>13</sup> reported an on-line method using a fibre optic coupled probe to monitor the  $p\text{H}_2$  fraction in a  $\text{H}_2$  moderator used for a neutron source. However, they reported relatively long analysis times of around 20 min per measurement.

Here we report that by using a Raman spectrometer fitted with a non-contact optic, with a backscattering  $180^\circ$  geometry, the acquisition of Raman spectra of  $\text{H}_2$  gas from the in-house built  $p\text{H}_2$  generator can be greatly simplified. This allows Raman spectra from at-line samples to be easily acquired using existing infrastructure (i.e. conventional NMR tubes). Also, this configuration allows the facile set-up of an on-line method of monitoring the performance of the generator, by focussing the laser onto a simple glass flow tube in the flow path of the generator. The rapid nature of the Raman procedure (every 30 s) enables in-situ monitoring of the fast back conversion of  $p\text{H}_2$  to  $n\text{H}_2$  inside contaminated NMR tubes.

## Experimental

At-line and on-line Raman analysis was used to characterise an in-house built  $p\text{H}_2$  generator, the schematic of which is shown in Figure 1.  $n\text{H}_2$  gas with a room temperature equilibrium content of  $p\text{H}_2$  was produced from water using a hydrogen generator (HG) electrolysis cell (Peak Scientific), operating at 4 bar for at-line experiments and 5 bar for on-line experiments. The  $n\text{H}_2$  gas then flowed into a two-way valve (V1), which directed the gas into either a chamber for enrichment of the  $p\text{H}_2$  content or directly into the rest of the system. The chamber for the enrichment of  $p\text{H}_2$  content was of similar design to that reported previously in the literature.<sup>4,27</sup> Briefly, it consisted of a copper coil (C) (OD = 9.5 mm, ID = 7.7 mm, L = 3 m) packed with charcoal (Sigma-Aldrich), which was submerged in a Dewar (D) filled with liquid nitrogen. The charcoal was held in place with

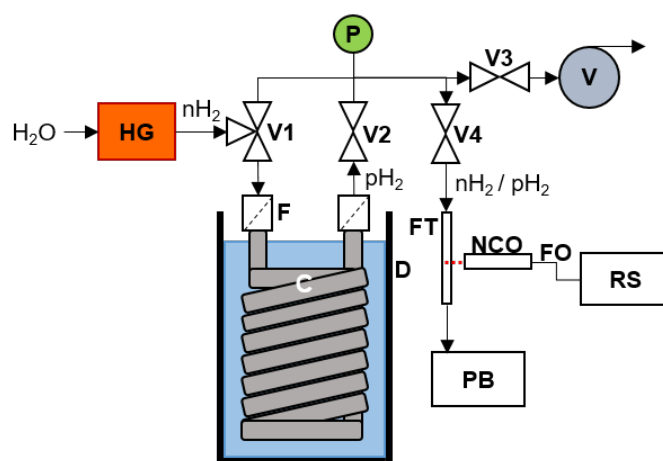


**Figure 1.** Schematic of the in-house built  $p\text{H}_2$  generator.  $\text{H}_2$  gas at 4 bar for at-line experiments, or 5 bar for on-line experiments (as shown in figure), was produced from water using a hydrogen generator (HG) electrolysis cell. The gas flowed into a two-way valve (V1), which directed the gas into either a chamber for enrichment of the  $p\text{H}_2$  content or directly into the rest of the system. The chamber for the enrichment of  $p\text{H}_2$  content is a copper coil (C) (OD = 9.5 mm, ID = 7.7 mm, L = 3 m) packed with charcoal, which was submerged in a Dewar (D) filled with liquid nitrogen. The charcoal was held in place with two  $40 \mu\text{m}$  in-line filters (F) at either end of the coil. On-off valves (V2, V3, V4) were used to control whether  $n\text{H}_2$  or  $p\text{H}_2$  enriched gas was provided to the outlet of V4. The system pressure was measured using a pressure transducer (P). A vacuum pump (V) was used to allow the system (and any connected flow tube or NMR tube) to be evacuated of gas.

two  $40 \mu\text{m}$  in-line filters (F) at either end of the coil. On-off valves (V2, V3, V4) were used to control whether  $n\text{H}_2$  or  $p\text{H}_2$  enriched gas was provided to the outlet of V4. The system was equipped with a pressure transducer (P) (Omega) to check the pressure of the gas, and also a vacuum pump (V) (Vacubrand, ultimate vacuum of 7 mbar) to allow the system (and any connected flow tube or NMR tube) to be evacuated of gas.

At the start of each experiment, the copper coil was filled with  $\text{H}_2$  to the desired pressure without being cooled. The coil was then purged so that the pressure was just above atmospheric, and filled again to ensure that only  $\text{H}_2$  gas was entering the system. The coil was then cooled with liquid nitrogen, and the purge process repeated. Once the pressure in the coil had again reached the desired level (usually after around 15 min), this was regarded as the start of the generator running time.

For at-line Raman analysis, the outlet of V4 was connected to a standard NMR tube (Wilma Precision, 527-PP-7) equipped with a Young's valve (GPE Scientific) (not shown in Figure 1). For on-line analysis, V4 was connected to a flow tube (FT) which had a 40 mm section of the same type of NMR tube partway along its length. The outlet of the flow tube was connected to a pneumatic control unit (Bruker) for a polariser box (PB) (as shown in Figure 1), which controlled when gas flowed along the FT into the PB and then out into the atmosphere. The PB was used to allow gas to flow for 15 s, with a desired interval (typically around every 5 min) between each flow duration. Between intervals, the PB held the gas pressure constant at 5 bar in the FT. The polariser

box has previously been used to automate SABRE NMR experiments,<sup>19,20,28,29</sup> but in this case it was simply used to control the flow of gas out of the pH<sub>2</sub> generator.

The Raman spectrometer (RS) used to record the spectra of the gas samples was a RamanRxn1 analyser (Kaiser Optical Systems), which utilised a CW diode laser with a maximum output of 400 mW at 785 nm. The axial transmissive spectrograph (f/1.8) was equipped with a holographic transmission grating (HoloPlex). The detector was a charged coupled device cooled to  $-40^{\circ}\text{C}$  (Peltier cooling). The spectral range was  $100\text{ cm}^{-1}$  to  $3425\text{ cm}^{-1}$  (Raman shift) with an average spectral resolution of  $4\text{ cm}^{-1}$ . The spectrometer was coupled with a 5 m fibre optic (FO) cable to a filtered MR Probe fitted with a non-contact optic (NCO). This NCO was used to focus the laser onto the centre of the NMR tube for at-line or in-situ analysis, or the centre of the NMR tube section within the FT for on-line analysis. The same optic was used to collect the backscattered light ( $180^{\circ}$  geometry) from the sample. The NCO had a 10 mm focal length and the size of the focused beam was approximately  $100\text{ }\mu\text{m}$  at the focal point. The laser power was around 270 mW at the sample. The spectrometer was calibrated with a neon atomic line source and a NIST traceable white light source for wavelength and intensity accuracy respectively. The calibration was verified using a cyclohexane standard prior to any analysis. A single scan with an integration time of 25 s was used for each spectrum. A dark spectrum, also of 25 s, was recorded before each scan and used for dark correction, giving a total acquisition time of around 50 s. For the experiments studying the stability of pH<sub>2</sub> in an NMR tube using a sampling frequency of 30 s, a single dark spectrum was recorded just before presenting the tube to the laser, and used to correct all of the recorded spectra for that sample.

Immediately after recording the at-line Raman spectrum of H<sub>2</sub> contained in a standard NMR tube, the <sup>1</sup>H NMR spectrum was also recorded in a method similar to that reported previously.<sup>15,16,21,27</sup> The sample was placed in a bench-top NMR spectrometer (Magritek Spinsolve) operating at a <sup>1</sup>H Larmor frequency of 43.5 MHz. A spectrum was recorded using a standard  $90^{\circ}$  pulse and detect sequence, with a bandwidth of 200 kHz, and 512 points per free induction decay (acquisition time of 2.56 ms) zero filled to 2048 points. A repetition time of 300 ms was used between scans. This duration is sufficiently larger than the  $T_1$  of oH<sub>2</sub>, which is reported as being between 3 ms and 15 ms,<sup>27</sup> to allow for quantitative analysis. 256 scans were acquired, resulting in an total acquisition time of 77 s.

All data analysis was conducted in the R programming environment.<sup>30</sup> The hyperSpec package<sup>31</sup> was used to load the Raman data, and the robust baseline correction algorithm provided by the baseline package<sup>32</sup> (with a span setting of 0.1) was used to remove the influence of the glass background in the Raman spectra.

## Results and Discussion

### Raman Spectra of Hydrogen Gas

Gas analysis by Raman spectroscopy can be challenging, because the small scattering cross-sections and low densities of the molecules in the gas phase lead to weak Raman

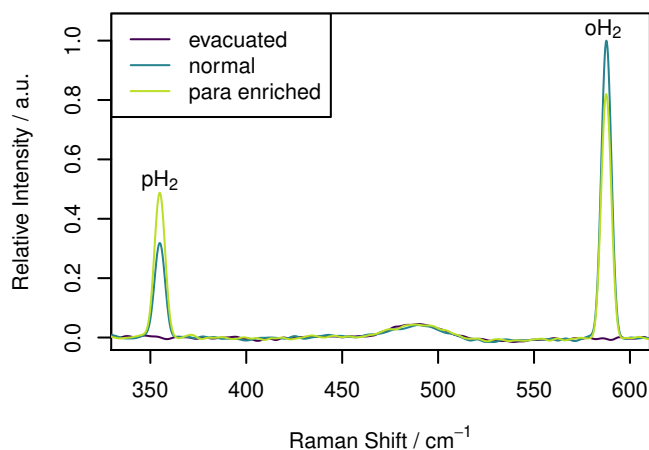


**Figure 2.** Raman spectra of an evacuated NMR tube, a tube filled with nH<sub>2</sub> at 4 bar, and a tube filled with pH<sub>2</sub> enriched H<sub>2</sub> at 4 bar.

signals.<sup>33–35</sup> Therefore, to confirm if sufficient signal could be obtained using our Raman set-up, the spectra from an evacuated NMR tube ( $\approx 7\text{ mbar}$ ), a tube filled to 4 bar with H<sub>2</sub> gas directly from the hydrogen generator (i.e. nH<sub>2</sub>), and a tube filled to 4 bar from the pH<sub>2</sub> generator after it had been running for 2 h were compared. The resulting spectra are shown in Figure 2. From this figure, it can be seen that peaks for the first two rotational bands of hydrogen at the expected Raman shifts of  $355\text{ cm}^{-1}$  and  $586\text{ cm}^{-1}$  are clearly visible in the spectra of the two gas samples. These correspond to the rotational transitions  $S_0(0)$  ( $J = 0 \rightarrow 2$ ) and  $S_0(1)$  ( $J = 1 \rightarrow 3$ ). Two further much weaker bands at  $812\text{ cm}^{-1}$  and  $1032\text{ cm}^{-1}$  were also observed (see Figure S1 in the supplementary information), corresponding to the transitions  $S_0(2)$  ( $J = 2 \rightarrow 4$ ) and  $S_0(3)$  ( $J = 3 \rightarrow 5$ ) respectively.<sup>25,36</sup> Higher rotational levels were not observed because these levels are not significantly populated at room temperature.<sup>3,36</sup> From the spectrum of the evacuated tube it can be seen that sampling through the glass wall of the NMR tube does not complicate the spectrum in this region, except with a broad glass signal which can be easily removed with baseline correction (see Figure S1 for examples of non-baseline correct spectra). As expected, the spectrum from the pH<sub>2</sub> enriched sample had a much greater proportion of signal from the rotational band corresponding to the pH<sub>2</sub> isomer, compared to the spectrum from the nH<sub>2</sub> sample.

As pH<sub>2</sub> and oH<sub>2</sub> isomers occupy different rotational energy levels, with pH<sub>2</sub> occupying even values of  $J$  (0, 2, ...) and oH<sub>2</sub> occupying odd values of  $J$  (1, 3, ...),<sup>1,3,4,37</sup> the ratio of these bands can be used to determine the para:ortho ratio.<sup>25</sup> Here we used the same calculation method as reported by Matthews et al.<sup>8,26</sup> Briefly, the Raman scattering intensities,  $I_J$ , of the rotational bands of H<sub>2</sub> are given by Eq. 1

$$I_J = \frac{(J+1)(J+2)}{(2J+1)(2J+3)} x_J p_J \gamma_J^2 \omega_s^3 \quad (1)$$

where  $x_J$  is the fraction of gas at the  $J^{\text{th}}$  level,  $p_J$  is the Boltzmann population of the  $J^{\text{th}}$  level at the measurement temperature,  $\gamma_J$  is the anisotropy of the polarizability tensor, and  $\omega_s$  is the scattered light angular frequency. Therefore, the ratio of the areas of the first two rotational bands ( $I_0$  and

$I_1$  at  $355\text{ cm}^{-1}$  and  $586\text{ cm}^{-1}$ , respectively) can be used to calculate the ratio of  $x_0$  and  $x_1$ , and hence the para:ortho ratio,  $r$ , as shown by Eq. 2.

$$r = \frac{x_0}{x_1} = \frac{3I_0p_1\gamma_1^2}{5I_1p_0\gamma_0^2} \quad (2)$$

This can be simply rearranged to give the p $H_2$  fraction,  $x_{pH_2}$ , as shown by Eq. 3.

$$x_{pH_2} = \frac{r}{1+r} \quad (3)$$

$p_J$  must be considered, as not all p $H_2$  molecules will occupy the  $J = 0$  ground rotational energy level (likewise not all o $H_2$  molecules will occupy  $J = 1$ ) at the measurement temperature (294 K).<sup>1,3,37</sup> Values for  $p_J$  were calculated using Boltzmann's distribution law,<sup>1,3</sup> with a rotational temperature of hydrogen,  $\theta_R$ , of 87.6 K.<sup>3,38</sup> The values reported by Hunt et al.,<sup>39</sup> were used for  $\gamma_J$ .

Using this method,  $x_{pH_2}$  for the Raman spectrum of the n $H_2$  sample shown in Figure 2 was calculated as being 25.6%. This value is very close to the expected equilibrium value of 25.1% for  $H_2$  at 294 K. Equilibrium values of  $x_{pH_2}$  can be calculated using Boltzmann statistics.<sup>1,3,11</sup> For the p $H_2$  enriched sample,  $x_{pH_2}$  was calculated as being 39.5%. Whilst this shows some enrichment over the n $H_2$  sample, the enrichment is much lower than the 52.1% expected at the 77 K operating temperature of the p $H_2$  generator. This discrepancy could be due to the generator requiring more than 2 h to reach its maximum  $x_{pH_2}$  output, or because conversion of p $H_2$  back to o $H_2$  is occurring inside the NMR tube. These two issues are explored below.

### At-line and On-line Monitoring of Generator Performance

Normally it is assumed that when  $H_2$  gas is passed over a catalyst, such as the charcoal used here, that the thermodynamic equilibrium position is obtained rapidly, usually within a few minutes.<sup>4,11,40</sup> However, as discussed above, it appears that the generator used here requires considerably longer to reach the equilibrium  $x_{pH_2}$  at its operating temperature. To investigate how long the p $H_2$  generator takes to reach steady state, a series of at-line samples of  $H_2$  gas were taken for Raman analysis over an 8 h time period. The analysis was repeated on several different days to check for consistency of performance. The results are presented in Figure 3, which shows that the p $H_2$  fraction gradually increases from around 32% to around 43.5% within 2 h. After 2 h the increase in  $x_{pH_2}$  begins to flatten out, and it takes over 8 h before a fairly steady production of around 50% is achieved. From Figure 3 it can also be seen that the generator performs similarly over several different days of operation, with some scatter caused possibly by different operating conditions in the laboratory (e.g. the room temperature which will effect the temperature of the  $H_2$  gas entering the conversion chamber). The data from each separate day of operation can be fitted to the exponential function given in Eq. 4,

$$x_{pH_2}(t) = \left[ x_{pH_2}(0) - x_{pH_2}^f \right] \exp\left(\frac{-t}{\tau}\right) + x_{pH_2}^f \quad (4)$$

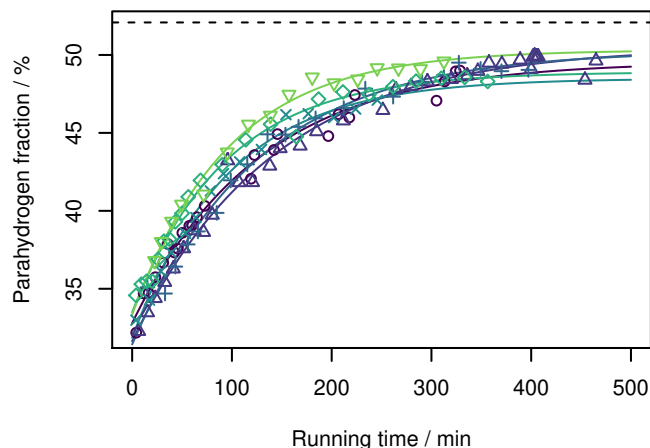


**Figure 3.** Plots of parahydrogen fraction ( $x_{pH_2}$ ) against generator running time for experiments conducted on six different days (different symbol shapes and colours). Samples were taken for Raman analysis by filling NMR tubes with p $H_2$  enriched  $H_2$  at 4 bar. The black horizontal dashed line shows the equilibrium value  $x_{pH_2}$  at the generator operating temperature (77 K). The solid lines show the fits of the data points from each day to the exponential function Eq. 4 (details in the main text and Table S1).

where  $x_{pH_2}(t)$  is the p $H_2$  fraction at time  $t$ ,  $x_{pH_2}(0)$  is the p $H_2$  fraction at time zero,  $\tau$  is a time constant, and  $x_{pH_2}^f$  is the final p $H_2$  fraction as time approaches infinity. Values between 94 min and 142 min, between 31.4% and 33.5%, and between 48.5% and 50.5% were estimated for  $\tau$ ,  $x_{pH_2}(0)$ , and  $x_{pH_2}^f$  respectively using non-linear least squares regression (see Table S1 for full details). One possible reason why  $x_{pH_2}^f$  does not reach the equilibrium value of 52.1% expected for p $H_2$  fraction at liquid nitrogen temperatures, is that the gas flowing through the coil does not reach 77 K due to insufficient cooling. A value of 50.0% for  $x_{pH_2}^f$ , instead suggests a slighter higher temperature of 80 K.

Gamliel et al.<sup>27</sup> also used a liquid nitrogen cooled p $H_2$  generator (although with an iron(III) oxide catalyst), and used NMR spectroscopy to measure  $x_{pH_2}$  of the resulting enriched gas. They reported a slow increase in  $x_{pH_2}$  over time, with 42.3% reached after around 2 h, increasing to 46.3% after 3.7 h. This is broadly similar to the rate of increase shown in Figure 3. They also report that the increase in  $x_{pH_2}$  is not linear with time, although they do not specify the form of the non-linear behaviour.

To monitor the performance of the p $H_2$  generator on-line a simple glass tube was inserted between the outlet of the generator and the inlet of a pneumatic control unit, as shown in Figure 1. This control unit is normally used to control the input of p $H_2$  into a mixing chamber used for hyperpolarisation experiments.<sup>19,20,28</sup> In this case the pneumatic control was used to regulate the pressure in the flow tube, and to control the flow of gas out of the p $H_2$  generator. The Raman laser was focussed onto the inside of the glass tube to provide in-situ analysis of the composition of the  $H_2$  gas flowing directly out of the generator and into the control unit.

Figure 4 shows the result of the calculated values of  $x_{pH_2}$  from the on-line Raman monitoring of the generator output. For the first 7 h of running time (before point A on Figure 4),

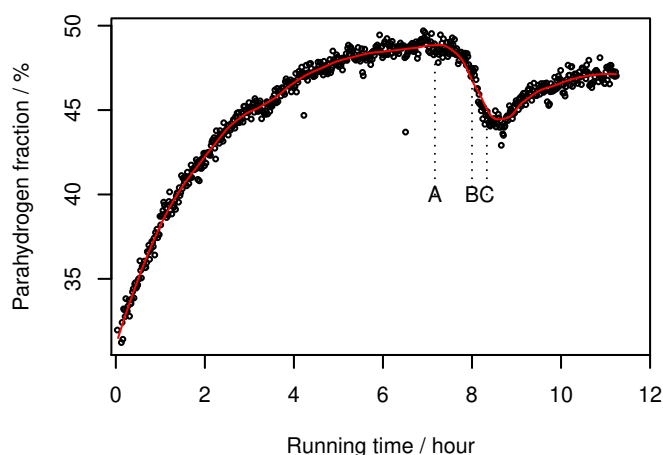


**Figure 4.** Plots of  $x_{pH_2}$  against time for the in-house built  $pH_2$  generator.  $x_{pH_2}$  was calculated from on-line Raman measurements of the gas flowing at 5 bar between the generator and a pneumatic control unit. Raman spectra were recorded every 60 s. The control unit was set to take 15 s samples of  $H_2$  every 340 s before point A, every 160 s between points A and B, every 100 s between points B and C, and every 220 s after point C. The solid line is a local polynomial regression (loess) fitting through the data, calculated using a span of 0.2.

the pneumatic control unit was set to sample  $H_2$  every 340 s. A sample by the pneumatic control unit consisted of a flow of gas regulated down from 5 bar to 4 bar for 15 s. As can be seen from Figure 4,  $x_{pH_2}$  increases from around 30% to 40% within the first 4 h, and a further 2 h is then required to reach 48%. This trend is similar to the case when at-line sampling was used (see Figure 3).

The sampling frequency used in hyperpolarisation studies that also use a similar pneumatic control unit is reported as being between 10 s to 45 s,<sup>20,28,41</sup> which is much more rapid than the once per 340 s used here. Therefore, after reaching steady state, the performance of the  $pH_2$  generator was tested by increasing the sampling frequency of the pneumatic control unit to once every 160 s (between points A and B on Figure 4), and then to once every 100 s (between points B and C on Figure 4). From Figure 4, it can be seen that  $x_{pH_2}$  decreases rapidly after point A. After point C, the sampling frequency was reduced to once every 220 s; after this point,  $x_{pH_2}$  gradually increases again back towards the maximum value of  $x_{pH_2}$ . As the pneumatic control unit regulates when flow occurs within the  $pH_2$  generator, a quicker sampling frequency results in a shorter residence time for the gas within the coil that contains the conversion catalyst, and hence less contact time for conversion from  $oH_2$  into  $pH_2$ . This explains why the  $x_{pH_2}$  decreases when the sampling frequency is too fast.

These results clearly show that the generator used here would not be suitable for use with very high sampling frequencies, as the  $x_{pH_2}$  would fluctuate depending on the resulting residence time. This important observation may have been missed without the use of rapid on-line monitoring. On-line monitoring could be used to judge the performance of any improved designs for the  $pH_2$  generator to make sure that performance is optimised and consistent. Possible improvements include: using various other catalyst

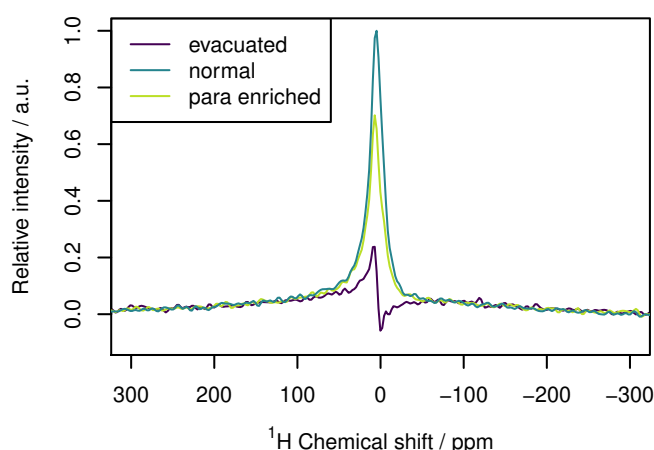


**Figure 5.** NMR spectra of an evacuated NMR tube, a tube filled with  $nH_2$  at 4 bar, and a tube filled with  $pH_2$  enriched  $H_2$  at 4 bar.

materials such as hydrous ferric oxide<sup>37</sup> instead of charcoal, increasing the submerged coil volume so that the residence time of the gas within the conversion chamber is increased, and increasing the surface area for heat transfer between the liquid nitrogen and the  $H_2$  gas on the surface of the catalyst.

### Comparison and Validation with NMR Measurements

To validate the Raman measurements, NMR analysis was also conducted on the  $pH_2$  enriched gas provided from the generator. As the samples taken for the at-line study with Raman were in standard NMR tubes, the exact same samples could be used for NMR analysis by simply inserting the sample into the bore of the NMR instrument. Here we used a bench-top NMR instrument ( $^1H$  frequency of 43.5 MHz). Whilst this provided less signal intensity than a high field instrument, it allowed the analysis to be conducted at-line; i.e., the  $pH_2$  generator, Raman spectrometer, and NMR spectrometer were all located within the same laboratory.

Quantification of  $x_{pH_2}$  in the gas phase by NMR can be challenging because of the low density of spins (e.g. compared to the liquid phase), and because  $pH_2$  is NMR silent.<sup>16</sup> However, the ortho isomer is NMR visible, and the  $x_{pH_2}$  can be calculated by taking the ratio of peak area from an unknown sample to that of a known sample (at the same gas density), usually  $nH_2$ .<sup>15,16,21,27</sup> Therefore, the NMR method only requires a single reference sample, and no further calibration is needed.

Figure 5 compares the NMR spectra of a tube filled with  $nH_2$  and  $pH_2$  enriched  $H_2$  at 4 bar. As expected, the signal is very broad<sup>16,27</sup> (around 100 ppm or 4350 Hz), and the area is lower for  $pH_2$  enriched gas. As can also be seen from the spectra of an evacuated NMR tube in Figure 5, there is a significant background signal. To correct for this, the background signal was subtracted from the spectra of the  $nH_2$  samples and the at-line samples (see Figure S2 for example corrected spectra), in a similar method to that reported by Hövener et al.<sup>16</sup>

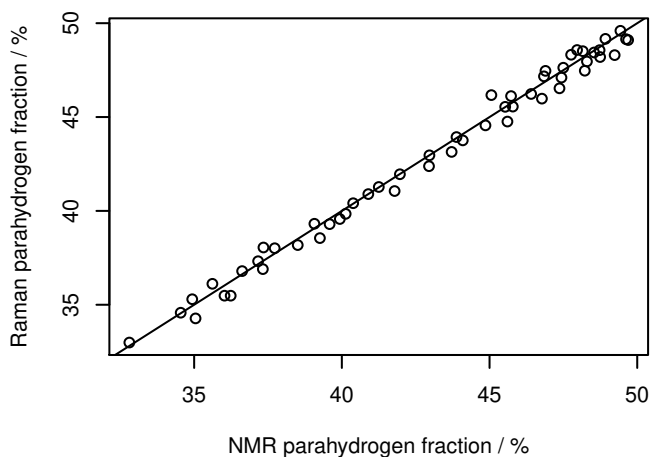


**Figure 6.** Plot of  $x_{pH_2}$  calculated using the Raman spectra, against  $x_{pH_2}$  calculated using the NMR spectra from the same at-line samples. The solid line shows the  $y = x$  line.

$x_{pH_2}$  was calculated from the at-line NMR spectra of  $H_2$  gas in the NMR tubes using Eq. 5.<sup>15</sup>

$$x_{pH_2} = 1 - x_{oH_2} \frac{S_0}{S_{ref}} \quad (5)$$

where  $S_0$  is the area of the  $oH_2$  peak in the NMR spectrum of an unknown sample, and  $S_{ref}$  is the area of the  $oH_2$  peak in the NMR spectrum of a sample with a known  $oH_2$  composition  $x_{oH_2}$ . An NMR tube filled with  $H_2$  directly from the hydrogen generator at 4 bar and 294 K was used as the reference sample. The tube was filled and measured five times to account for slight deviations in filling pressure, and the average area was used as the value for  $S_{ref}$ . Based on the measurement temperature,  $x_{oH_2}$  was calculated as 74.9%. Figure 6 shows the comparison of  $x_{pH_2}$  calculated from at-line samples using Raman and NMR analysis, and it can be seen that there is very good agreement between the two methods, with  $R^2 = 0.991$  and RMSE = 0.48%.

Although there is excellent agreement between the two measuring techniques, Raman analysis has several advantages over NMR for this application. The Raman technique does not require a reference sample, as both spin isomers can be directly detected, which simplifies the procedure and eliminates some sources of error. In NMR analysis,  $pH_2$  is only measured indirectly by measuring the change in the  $oH_2$  signal. Whilst accurate results can be achieved with the  $pH_2$  fractions analysed from the generator used in this work ( $x_{pH_2} < 52\%$ ), it would be more difficult to analyse higher  $pH_2$  fractions from a more efficiently cooled generator. This is because there is less  $oH_2$  signal to measure with NMR as the  $pH_2$  fraction increases. As NMR is an indirect method, it therefore requires a reference sample with a known composition of  $oH_2$ . An obvious choice is to use another tube filled with hydrogen that has a room temperature equilibrium composition of  $oH_2$  (i.e.  $nH_2$ ). Although this assumes that the reference and unknown samples are filled to the same density, i.e. the same temperature and pressure.<sup>15,21</sup> To avoid this problem, Feng et al.<sup>15</sup> also used the unknown sample as the reference sample, by waiting 72 h for the sample to return to the room temperature equilibrium composition of  $oH_2$ . However, this

assumes no leaking of the sample, and the method is not compatible with taking multiple samples in quick succession. Therefore, we used the approach of using a separate sample of  $nH_2$  as the reference, as used elsewhere.<sup>16,21,27</sup>

The temperature of the laboratory was measured with a standard kerosene-in-glass thermometer with an accuracy of  $\pm 1.5$  K, and the pressure of the gas in the tube was measured with a pressure transducer with an accuracy of  $\pm 0.008$  bar. Taking into account the density of  $H_2$ ,<sup>42</sup> this added an uncertainty of  $\pm 1.1\%$  to the values of  $x_{pH_2}$  measured by NMR. As the at-line samples were filled manually, the repeatability of pressure was only better than  $\pm 0.05$  bar between different samples. This resulted in an uncertainty of  $\pm 2.6\%$  to the values of  $x_{pH_2}$  (see Figure S3 for details). The Raman method is insensitive to changes in density between samples, because this changes the intensity of the peaks but not the ratio between the peaks. So an accurate result could be obtained as long as the filling density was high enough to provide sufficient signal.

Both the Raman and the NMR methods require calculation of the Boltzmann distribution between rotational energy levels of  $H_2$ , to calculate  $p_0$  and  $p_1$  in Eq. 2 for Raman, and to calculate  $x_{oH_2}$  in Eq. 5 for NMR. These calculations required the temperature of the gas to be measured. However, as the Boltzmann distribution only varies slowly around room temperature, this added an uncertainty of less than  $\pm 0.1\%$  for Raman analysis, and  $\pm 0.01\%$  for NMR analysis (see Figures S4 and S5 for details).

### *In-situ monitoring of the Conversion of $pH_2$ in NMR Tubes*

Conversion between  $oH_2$  and  $pH_2$  spin isomers is forbidden, so spontaneous gas phase conversion is very slow.<sup>3,5,37</sup> However, the glass wall of an NMR tube (e.g. as used for a SABRE hyperpolarisation experiment) offers a surface for the heterogeneous conversion between spin isomers, which is more rapid.<sup>15,37</sup> Various paramagnetic species in the glass wall (or in the sample) may also accelerate the conversion.<sup>37</sup> In fact, storage of samples under  $nH_2$  at liquid nitrogen temperatures prior to thawing and NMR detection led to one of the first reports of parahydrogen induced polarisation (PHIP), as  $pH_2$  enrichment was built up during sample storage.<sup>4,43,44</sup> Additionally, if there is an imperfect seal when filling the NMR tube, small amounts of oxygen could be introduced. This oxygen could then also act as a paramagnetic catalyst for the conversion of the spin isomers.<sup>21</sup>

Gamliel et al.<sup>27</sup> measured the conversion of  $pH_2$  in NMR tubes (type of glass not specified), using an NMR method similar to that described above to determine the  $pH_2$  fraction in the gas. They reported that no conversion of  $pH_2$  occurred, however they only monitored the samples for 20 min. Tom et al.<sup>21</sup> also measured the conversion of  $pH_2$  in NMR tubes using NMR to monitor the  $pH_2$  content. They reported that the back conversion to  $oH_2$  at room temperature for a sample starting with  $\approx 99.9\%$   $pH_2$  enrichment was  $0.4\% h^{-1}$  in tubes made from the same type of borosilicate glass as used here. Similarly Feng et al.<sup>15</sup> monitored the conversion of  $pH_2$  to  $oH_2$  every 8 min for 64 h in an NMR tube. They found that the conversion profile followed an exponential function with

a time constant of around 846 min. Hövener et al.<sup>16</sup> observed a similar profile in a borosilicate glass vial monitored over 41 h, again using NMR to determine the  $pH_2$  fraction; they reported a similar time constant of around 820 min.

To determine if conversion of  $pH_2$  to  $oH_2$  was occurring inside the NMR tubes used here, five different tubes were filled with  $H_2$  from the  $pH_2$  generator at 4 bar and then analysed with Raman spectroscopy every 30 s for 40 min. The sampling was done in a similar manner to the at-line study described above, except that the NMR tube was left in the beam path of the laser between measurements, resulting in an in-situ measurement of any conversion occurring inside the NMR tube. For three of the tubes it was found that almost no back-conversion occurred within 40 min. For instance, for one sample  $x_{pH_2}$  values were scattered around a mean of 40.5 %, with a total range of about 1 %, and a standard deviation of 0.3 % (see Figure S6). This indicates that good precision and repeatability can be achieved even with rapid sampling.

For two of the NMR tubes used, conversion from  $pH_2$  to  $oH_2$  occurred rapidly with a significant decrease in  $pH_2$  fraction within 40 min. To investigate this further, these two tubes were refilled with fresh  $pH_2$  to 4 bar and analysed every 30 s for 3 h. The results are shown in Figure 7, which shows that  $x_{pH_2}$  decreases very rapidly in both of these tubes, with complete conversion within 3 h and within 1 h for tubes 1 and 2 respectively. The two tubes that catalysed the  $pH_2$  to  $oH_2$  conversion had very reproducible behaviour. It was possible to fit an exponential to the decay of  $x_{pH_2}$  against time, where the fit had the same rate constant for each replicate experiment. The rate constant was  $5.3 \times 10^{-4} \text{ s}^{-1}$  for tube 1 and  $27.4 \times 10^{-4} \text{ s}^{-1}$  for tube 2. The reason for the vertical offset seen for tube 1 is that the tube was filled at different  $pH_2$  generator running times, and so had slightly different starting values of  $x_{pH_2}$ . This suggests that these tubes were contaminated with some form of impurity that accelerates the conversion of  $pH_2$  to  $oH_2$ .

These results show that by using in-situ Raman analysis it was possible to monitor a rapid reaction in the gas phase, which may have gone unnoticed with other analysis techniques. The results also highlight the need to check glassware used when working with  $pH_2$  enriched gas, as many different types of impurities can promote the back conversion to  $oH_2$ .<sup>2,5,37</sup>

To determine the long term stability of  $pH_2$  in a non-contaminated tube, a fresh sample was analysed every 20 min for a period of 18 h. This sample started with a  $x_{pH_2}$  of 43.0 % and decayed with a linear rate of  $0.08 \text{ \% h}^{-1}$  to 41.6 % (see Figure S7). This confirms that  $pH_2$  is very stable within the non-contaminated NMR tubes, and thus any conversion will have a negligible impact on the level of  $x_{pH_2}$  for the measurement times used in the at-line and on-line monitoring discussed above ( $\leq 50$  s).

## Conclusion

In this work, we have presented a rapid method to determine quantitatively the  $pH_2$  fraction in  $H_2$  gas using Raman spectroscopy. The Raman method has several advantages over other analytical techniques for determining  $pH_2$  fraction, most notably that no calibration samples are

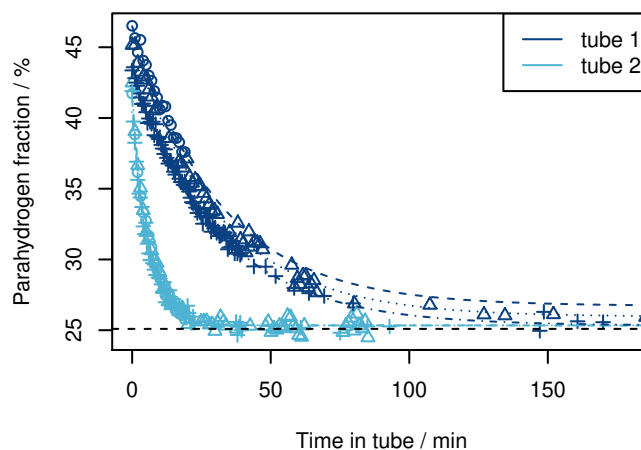


**Figure 7.** Plots of parahydrogen fraction ( $x_{pH_2}$ ) against time for two NMR tubes found to accelerate the conversion of  $pH_2$  to  $oH_2$ .  $x_{pH_2}$  was calculated from the in-situ Raman spectrum of  $pH_2$  enriched  $H_2$  gas at 4 bar. Time zero was regarded as the time that the sample was filled from the  $pH_2$  generator. Each colour indicates a different tube, and each symbol type is a different sample (refilled with fresh  $pH_2$  each time) in the tube. The coloured dashed and dotted lines show an exponential fit through the decay of  $x_{pH_2}$  against time (details in the main text). The black horizontal dashed line shows the equilibrium value  $x_{pH_2}$  at the measurement temperature.

required. Here we used a NCO to acquire Raman spectra of  $H_2$  gas at moderate pressures ( $\leq 5$  bar) from within standard NMR tubes or a glass flow tube. This approach greatly simplifies the set-up, and allows for much more rapid analysis compared to previous literature reports of using Raman spectroscopy to measure  $pH_2$  fraction.<sup>8,10,13,14,26</sup>

The performance of an in-house built  $pH_2$  generator was measured on-line by recording Raman spectra from a flow tube at the outlet of the generator. It was found that the generator required much longer than anticipated to reach steady state output (around 7 h). It was also found that increasing the flow rate of the gas within the generator reduces the enrichment achieved, presumably because of a reduction in residence time of the gas flowing in the generator. This result has important implications for hyperpolarisation experiments requiring  $pH_2$  such as SABRE, as the NMR signal enhancement achieved is proportional to the enrichment level of the  $pH_2$  gas used.<sup>4,11,15</sup> The on-line monitoring method reported here could be used in the future to correlate the enhancement of the NMR signal by SABRE to the  $pH_2$  fraction, and to assess any changes to the  $pH_2$  generator design.

The rapid nature of the analysis used here permitted Raman spectra to be acquired every 30 s, so that the fast interconversion of the spin isomers of hydrogen from an enriched composition back to the room temperature equilibrium fraction within contaminated NMR tubes could be followed in detail. This interconversion may have been unnoticed with other slower analytical methods. Our results reveal a clear challenge when working with what is predicted to be essentially identical NMR tubes. It is also vital to take note that many PHIP approaches use sealed NMR tubes, and often monitor product formation over minutes to

hours.<sup>4,11,45,46</sup> Significant care must therefore be taken in excluding sample preparation effects in such studies.

The results reported here for on-line and in-situ monitoring using commercially available hardware, represent close to a 500-fold increase in sensitivity compared to some previously reported work.<sup>13</sup> Improvement and customisation of the experimental set-up, e.g. by the use of multiple optical passes, could be expected to further increase the signal. More generally, this work demonstrates that Raman spectroscopy can be used to quantify the pH<sub>2</sub> fraction in H<sub>2</sub> gas in a fast and convenient manner. This is important in many other applications which require pH<sub>2</sub>, such as storage of H<sub>2</sub> for fuel.

### Acknowledgements

We thank Mr. Neil Hodgson for assistance constructing the pH<sub>2</sub> generator, Dr. Thomas McGlone for support with the initial testing of the Raman analysis of H<sub>2</sub> gas, and Dr. Charlotte Matheson for proofreading assistance.

### Declaration of conflicting interests

The authors report there are no conflicts of interest.

### Funding

This project was funded by EPSRC (EP/M020983/1).

### Supplemental material

All supplemental material mentioned in text is available in the online version of the journal at <http://www.xxxxx>. All experimental Raman and NMR data reported in this work is available via University of Strathclyde's KnowledgeBase at <http://dx.doi.org/xxxxx>.

### References

1. Farkas A. *Orthohydrogen, Parahydrogen and Heavy Hydrogen*. London: Cambridge University Press, 1935.
2. Matsumoto M and Espenson JH. Kinetics of the Interconversion of Parahydrogen and Orthohydrogen Catalyzed by Paramagnetic Complex Ions. *J Am Chem Soc* 2005; 127(32): 11447–11453. DOI:10.1021/ja0524292.
3. Green RA, Adams RW, Duckett SB et al. The theory and practice of hyperpolarization in magnetic resonance using parahydrogen. *Prog Nucl Magn Reson Spectrosc* 2012; 67: 1–48. DOI:10.1016/j.pnmrs.2012.03.001. URL <http://dx.doi.org/10.1016/j.pnmrs.2012.03.001>.
4. Natterer J and Bargon J. Parahydrogen Induced Polarization. *Prog Nucl Magn Reson Spectrosc* 1997; 31: 293–315.
5. Buntkowsky G, Walaszek B, Adamczyk A et al. Mechanism of nuclear spin initiated para-H<sub>2</sub> to ortho-H<sub>2</sub> conversion. *Phys Chem Chem Phys* 2006; 8(16): 1929–1935. DOI:10.1039/b601594h. URL <http://xlink.rsc.org/?DOI=b601594h>.
6. Sloop JL. *Liquid Hydrogen as a Propulsion Fuel, 1945-1959*. NASA History Series, CreateSpace Independent Publishing Platform, 2016. ISBN 1530123526. URL <https://history.nasa.gov/SP-4404/app-a3.htm>.
7. Baade WF, Parekh UN and Raman VS. *Hydrogen*. John Wiley & Sons, Inc. ISBN 9780471238966, 2000. DOI: 10.1002/0471238961.0825041803262116.a01.pub2. URL <http://dx.doi.org/10.1002/0471238961.0825041803262116.a01.pub2>.
8. Petitpas G, Aceves SM, Matthews MJ et al. Para-H<sub>2</sub> to ortho-H<sub>2</sub> conversion in a full-scale automotive cryogenic pressurized hydrogen storage up to 345 bar. *Int J Hydrogen Energy* 2014; 39(12): 6533–6547. DOI:10.1016/j.ijhydene.2014.01.205. URL <http://dx.doi.org/10.1016/j.ijhydene.2014.01.205>.
9. Tam S and Fajardo ME. Ortho/para hydrogen converter for rapid deposition matrix isolation spectroscopy. *Rev Sci Instrum* 1999; 70(4): 1926–1932. DOI:10.1063/1.1149734. URL <http://aip.scitation.org/doi/10.1063/1.1149734>.
10. Sundararajan K, Sankaran K, Ramanathan N et al. Production and characterization of para-hydrogen gas for matrix isolation infrared spectroscopy. *J Mol Struct* 2016; 1117: 181–191. DOI:10.1016/j.molstruc.2016.03.068. URL <http://dx.doi.org/10.1016/j.molstruc.2016.03.068>.
11. Kuhn LT (ed.) *Hyperpolarization Methods in NMR Spectroscopy*. Number 338 in Topics in Current Chemistry, Heidelberg: Springer, 2013.
12. Duckett SB and Mewis RE. Application of Parahydrogen Induced Polarization Techniques in NMR Spectroscopy and Imaging. *Acc Chem Res* 2012; 45(8): 1247–57. DOI:10.1021/ar2003094. URL <http://pubs.acs.org/doi/abs/10.1021/ar2003094>{%}5Cnhttp://www.ncbi.nlm.nih.gov/pubmed/22452702.
13. Sutherland LM, Knudson JN, Mocko M et al. Practical in-situ determination of ortho-para hydrogen ratios via fiber-optic based Raman spectroscopy. *Nucl Instrum Methods Phys Res, Sect A* 2016; 810: 182–185. DOI:10.1016/j.nima.2015.12.009. URL <http://dx.doi.org/10.1016/j.nima.2015.12.009>.
14. Teshigawara M, Harada M, Tatsumoto H et al. Experimental verification of equilibrium para-hydrogen levels in hydrogen moderators irradiated by spallation neutrons at J-PARC. *Nucl Instrum Methods Phys Res, Sect B* 2016; 368: 66–70. DOI: 10.1016/j.nimb.2015.12.023. URL <http://dx.doi.org/10.1016/j.nimb.2015.12.023>.
15. Feng B, Coffey AM, Colon RD et al. A pulsed injection parahydrogen generator and techniques for quantifying enrichment. *J Magn Reson* 2012; 214: 258–262. DOI: 10.1016/j.jmr.2011.11.015. URL <http://dx.doi.org/10.1016/j.jmr.2011.11.015>.
16. Hövener JB, Bär S, Leupold J et al. A continuous-flow, high-throughput, high-pressure parahydrogen converter for hyperpolarization in a clinical setting. *NMR Biomed* 2013; 26(2): 124–131. DOI:10.1002/nbm.2827.
17. Bruker. Parahydrogen generator. <https://www.bruker.com/products/mr/nmr/accessories/hyperpolarization/parahydrogen-generator/overview.html>. Accessed 2018-07-27.
18. Halse ME. Perspectives for hyperpolarisation in compact NMR. *TrAC, Trends Anal Chem* 2016; 83: 76–83. DOI: 10.1016/j.trac.2016.05.004. URL <http://dx.doi.org/10.1016/j.trac.2016.05.004>.
19. Richardson PM, Jackson S, Parrott AJ et al. A simple hand-held magnet array for efficient and reproducible SABRE hyperpolarisation using manual sample shaking. *Magn Reson Chem* 2018; 56: 641–650. DOI:10.1002/mrc.4687. URL <http://doi.wiley.com/10.1002/mrc.4687>.

20. Richardson PM, Parrott AJ, Semenova O et al. SABRE hyperpolarization enables high-sensitivity  $^1\text{H}$  and  $^{13}\text{C}$  benchtop NMR spectroscopy. *Analyst* 2018; 143: 3442–3450. DOI:10.1039/c8an00596f.
21. Tom BA, Bhasker S, Miyamoto Y et al. Producing and quantifying enriched para-  $\text{H}_2$ . *Rev Sci Instrum* 2009; 80(1): 016108. DOI:10.1063/1.3072881.
22. Sakoda N, Shindo K, Shinzato K et al. Review of the thermodynamic properties of hydrogen based on existing equations of state. *Int J Thermophys* 2010; 31(2): 276–296.
23. Leachman JW, Jacobsen RT, Penoncello SG et al. Fundamental Equations of State for Parahydrogen, Normal Hydrogen, and Orthohydrogen. *J Phys Chem Ref Data* 2009; 38(3): 721–748. DOI:10.1063/1.3160306. URL <https://doi.org/10.1063/1.3160306>. <https://doi.org/10.1063/1.3160306>.
24. Bradshaw TW and Norris JOW. Observations on the use of a thermal conductivity cell to measure the para hydrogen concentration in a mixture of para and ortho hydrogen gas. *Rev Sci Instrum* 1987; 58(1): 83–85. DOI:10.1063/1.1139519.
25. Fleury PA and McTague JP. Molecular interactions in the condensed phases of ortho-para hydrogen mixtures. *Phys Rev A* 1975; 12(1): 317–326. DOI:10.1103/PhysRevA.12.317.
26. Matthews MJ, Petitpas G and Aceves SM. A study of spin isomer conversion kinetics in supercritical fluid hydrogen for cryogenic fuel storage technologies. *Appl Phys Lett* 2011; 99(8): 1–4. DOI:10.1063/1.3628453.
27. Gamliel A, Allouche-Arnon H, Nalbandian R et al. An Apparatus for Production of Isotopically and Spin-Enriched Hydrogen for Induced Polarization Studies. *Appl Magn Reson* 2010; 39(4): 329–345. DOI:10.1007/s00723-010-0161-9.
28. Mewis RE, Atkinson KD, Cowley MJ et al. Probing signal amplification by reversible exchange using an NMR flow system. *Magn Reson Chem* 2014; 52(February): 358–369. DOI:10.1002/mrc.4073.
29. Lloyd LS, Adams RW, Bernstein M et al. Utilization of SABRE derived hyperpolarization to detect low concentration analytes via 1D- and 2D-NMR methods. *J Am Chem Soc* 2012; 134: 12904–12907. DOI:10.1021/ja3051052. URL <http://dx.doi.org/10.1021/ja3051052>.
30. R Core Team. *R: A Language and Environment for Statistical Computing*. R Foundation for Statistical Computing, Vienna, Austria, 2017. URL <https://www.R-project.org/>.
31. Beleites C and Sergio V. *hyperSpec: a package to handle hyperspectral data sets in R*, 2016. URL <http://hyperspec.r-forge.r-project.org>. R package version 0.98-20161118.
32. Liland KH and Mevik BH. *baseline: Baseline Correction of Spectra*, 2015. URL <https://CRAN.R-project.org/package=baseline>. R package version 1.2-1.
33. Petrov DV and Matrosov II. Raman Gas Analyzer (RGA): Natural Gas Measurements. *Appl Spectrosc* 2016; 70(10): 1770–1776. DOI:10.1177/0003702816644611.
34. Petrov DV and Matrosov II. Pressure dependence of the Raman signal intensity in high-pressure gases. *J Raman Spectrosc* 2017; 48: 474–478. DOI:10.1002/jrs.5062.
35. Kiefer J. Recent advances in the characterization of gaseous and liquid fuels by vibrational spectroscopy. *Energies* 2015; 8: 3165–3197. DOI:10.3390/en8043165.
36. Eichmann SC, Weschta M, Kiefer J et al. Characterization of a fast gas analyzer based on Raman scattering for the analysis of synthesis gas. *Rev Sci Instrum* 2010; 81(12): 125104. DOI: 10.1063/1.3521397.
37. Ilicsa E. Ortho-para conversion of hydrogen molecules physisorbed on surfaces. *Prog Surf Sci* 1992; 41: 217–335. DOI:10.1016/0079-6816(92)90019-E.
38. Atkins PW and de Paula J. *Atkins' physical chemistry*. 9 ed. Oxford: Oxford University Press, 2010.
39. Hunt JL, Poll JD and Wolniewicz L. Ab initio calculation of properties of the neutral diatomic hydrogen molecules  $\text{H}_2$ , HD, D $_2$ , HT, DT, and T $_2$ . *Can J Phys* 1984; 62: 1719–1723. URL <papers2://publication/uuid/D6E1726A-39FA-45B7-A6E6-867696427946>.
40. Duckett SB and Sleigh CJ. Applications of the parahydrogen phenomenon: A chemical perspective. *Prog Nucl Magn Reson Spectrosc* 1999; 34(1): 71–92. DOI:10.1016/S0079-6565(98)00027-2.
41. Reile I, Aspers RLEG, Tyburn JM et al. DOSY Analysis of Micromolar Analytes: Resolving Dilute Mixtures by SABRE Hyperpolarization. *Angew Chem, Int Ed* 2017; 56: 9174–9177. DOI:10.1002/anie.201703577.
42. Lemmon EW, McLinden MO and Friend DG. *NIST Chemistry WebBook, NIST Standard Reference Database Number 69*, chapter Thermophysical Properties of Fluid Systems. National Institute of Standards and Technology, 2018. DOI:10.18434/T4D303.
43. Eisenberg R. Parahydrogen-Induced Polarization: A New Spin on Reactions with  $\text{H}_2$ . *Acc Chem Res* 1991; 24(4): 110–116. DOI:10.1021/ar00004a004.
44. Eisenschmid TC, Kirss RU, Deutsch PP et al. Para Hydrogen Induced Polarization in Hydrogenation Reactions. *J Am Chem Soc* 1987; 109(26): 8089–8091. DOI:10.1021/ja00260a026.
45. Blazina D, Duckett SB, Dunne JP et al. Applications of the parahydrogen phenomenon in inorganic chemistry. *Dalton Trans* 2004; : 2601–2609 DOI:10.1039/B409606A. URL <http://dx.doi.org/10.1039/B409606A>.
46. Duckett SB and Wood NJ. Parahydrogen-based NMR methods as a mechanistic probe in inorganic chemistry. *Coord Chem Rev* 2008; 252(21-22): 2278–2291. DOI:10.1016/j.ccr.2008.01.028.